Available online at www.sciencedirect.com

ScienceDirect

Procedia CIRP 113 (2022) 576–581

www.elsevier.com/locate/procedia

ISEM XXI

Femtosecond laser processing of cemented carbide for selective removal of cobalt

Balasubramanian Nagarajan[a,*], Jide Han[a], Shuigen Huang[b], Jun Qian[a], Jozef Vleugels[b], Sylvie Castagne[a]

[a]*Department of Mechanical Engineering and Flanders Make@KU Leuven-MaPS, KU Leuven, 3001 Leuven, Belgium*
[b]*Department of Materials Engineering, KU Leuven, 3001 Leuven, Belgium*

* Corresponding author. Tel.: +32-16-32 67 20. *E-mail address:* balasubramanian.nagarajan@kuleuven.be

Abstract

Diamond coating of tungsten carbide-cobalt (WC-Co) cemented carbide tools using chemical vapour deposition (CVD) requires removal of the cobalt (Co) binder phase from the WC-Co surface in order to improve the coating adhesion. Laser ablation is shown to be a promising technique for the selective phase removal of Co, which is based on the difference in melting and boiling temperatures between the different phases. However, laser ablation with conventional nanosecond (*ns*) laser pulses typically induces surface remelting, incomplete Co removal, and metallurgical changes in the WC phase due to the large heat-affected zone (HAZ) involved. Ultrashort pulsed lasers have emerged as an alternative due to minimized HAZ and thermal stresses, enabling cold ablation. This paper reports on the effect of femtosecond (*fs*) laser ablation on the selective removal of Co from polished WC-Co surfaces. The influence of several process variables including laser pulse energy, number of pulses, and scanning speed on the surface morphology of the *fs*-laser ablated surfaces was investigated. Two different WC-Co grades with 6% and 10% wt Co binder and different WC grain sizes were examined in this study. A pulsed ytterbium fiber laser (250 *fs*, 1030 nm) was used for the laser ablation of different morphologies such as spots, lines, and square regions. Field emission scanning electron microscopy (FESEM) and energy-dispersive X-ray (EDX) analysis were used to characterize the microstructure and chemical composition of the processed surfaces. The experimental results indicated that *fs* laser processing at optimized processing parameters could achieve successful removal of the Co phase selectively from the WC-Co surface with minimized morphological changes or thermal effects on the WC grains.

© 2022 The Authors. Published by Elsevier B.V.
This is an open access article under the CC BY-NC-ND license (https://creativecommons.org/licenses/by-nc-nd/4.0)
Peer-review under responsibility of the scientific committee of the ISEM XXI

Keywords: Femtosecond laser processing, selective phase removal, cemented tungsten carbide, diamond coating

1. Introduction

Cemented tungsten carbide-cobalt (WC-Co) is one of the common materials for cutting tool applications due to its desirable wear-resistant characteristics. WC-Co tools are commonly coated by physical vapour deposition (PVD) or chemical vapour deposition (CVD) with a wide range of materials, such as diamond, for better performance and durability [1]. However, during CVD of diamond, graphitization occurs at the diamond-carbide interface due to the high solubility and diffusivity of carbon in Co under the deposition conditions, which is detrimental to the quality of the diamond coatings [2]. Therefore, the Co phase needs to be removed from the WC-Co surface for an effective diamond coating, which is commonly performed by (electro)chemical etching [3]. The etching process generally consists of a two-step sequence to successively remove WC and Co. However, chemical etching is shown to cause detachment of large grains and corrugation of WC grains, while over-etching of Co can lead to subsurface porosity by pitting corrosion [4,5]. The porous grain boundaries of WC after etching reduce the

2212-8271 © 2022 The Authors. Published by Elsevier B.V.
This is an open access article under the CC BY-NC-ND license (https://creativecommons.org/licenses/by-nc-nd/4.0)
Peer-review under responsibility of the scientific committee of the ISEM XXI
10.1016/j.procir.2022.09.177

toughness, which further accelerates coating failure during the cutting process.

Alternatively, laser ablation is proposed as a promising technique for selective phase removal of Co from the WC-Co surface [6,7]. Li et al. [6] demonstrated selective removal of the Co binder from a WC-Co surface using a pulsed UV laser with 20 nanosecond (*ns)* pulse duration at optimum laser fluence and number of pulses where the resulting surface morphology was comprised of peaks (WC) and valleys (Co). However, WC grains were significantly affected in terms of grain growth, the disappearance of WC grain boundary sharpness and WC phase change to W_2C during laser ablation. Barletta et al. [7] used a continuous wave (CW) laser to fully remove Co from the surface but WC grain growth was observed in addition to the local partial melting of WC. Selective ablation of Co from WC-Co surface by laser ablation is based on the difference in melting point between the two phases, Co and WC. The melting and boiling temperatures of Co are 1768K and 3200K, respectively, compared to 3243K and 6273K for WC [7]. However, laser ablation by long pulsed lasers and CW lasers causes surface remelting, incomplete removal of Co, and metallurgical changes in the WC phase as the material removal mechanism is dominated by melting and vaporization involving large heat-affected zones (HAZ). All these effects are detrimental to the diamond coating adhesion and tool life [4].

Ultrashort pulsed lasers have been used in recent times for selective phase removal [8] which induces minimal thermal effects as the pulse duration [typically less than 10 picoseconds (*ps*)] is shorter than the electron-phonon relaxation time. Recently, Shiqi et al. [9] compared laser patterning of WC-Co surface using *ns*, *ps* and femtosecond (*fs*) laser pulses. Thermal diffusion was dominant during the *ns* laser ablation which resulted in Co binder vaporization and thermal residual stress leading to the formation of an oxide layer, cracks and pores on the WC surface. With *ps* lasers, ripples were formed on the WC grains whereas a cross-sectional analysis reveals that both Co binder and WC grains have been ablated at the center of the processing zone. Samples processed by a *fs* laser showed no defects at the subsurface but no obvious binder removal could be noticed [9,10]. However, the experiments were conducted on WC-Co grade with a coarse WC grain size (~ 20 µm) and 14 wt% Co, which is not desirable as a substrate for diamond coating applications.

This study focuses on the effect of *fs* laser processing (FLP) on the microstructure of WC-Co with ultrafine and medium WC grains (average grain size ~ 0.55 and 2.2 µm). The influence of various process parameters such as laser pulse energy, scanning speed and number of pulses on the microstructure and morphology of the *fs* laser processed surfaces is examined to identify the optimal process parameters for selective removal of the Co phase.

Nomenclature

FLP	Femtosecond laser processing
WC	Tungsten carbide
Co	Cobalt
ns	Nanosecond
ps	Picosecond
fs	Femtosecond
CW	Continuous wave
CVD	Chemical vapour deposition
PVD	Physical vapour deposition
FESEM	Field emission scanning electron microscopy
WDS	Wavelength dispersive X-ray spectroscopy
EPMA	Electron probe microanalysis
HAZ	Heat-affected zone
PO	Pulse overlap

2. Materials and methods

A WC-Co grade with 6 wt% Co and 1 µm WC grain size is typically preferred as substrate for the diamond coating to minimize the thermal stresses during CVD. In this study, two different grades of WC-Co with varying WC grain size and Co content, WC-6%wt Co (MG12, CERATIZIT**)** and WC-10%wt Co (GC32, CERATIZIT), were examined. The average grain size of MG12 and GC32 are 0.55 µm and 2.16 µm, respectively. Fig. 1 compares the backscattered electron microstructure of MG12 and GC32, showing the WC and Co phases as white and dark phases, respectively. The hardmetals were mechanically polished to mirror finish before *fs* laser processing.

FLP was conducted using a *fs* laser source with a Gaussian beam (SATSUMA, Amplitude Systèmes). The specification of the system is as follows: pulse duration (τ) = 250 *fs*, maximum average laser power = 10 W, maximum pulse energy (E_p) = 15.7 µJ, spot size (d_f) at $1/e^2$ intensity = 16 µm and focal length = 100 mm. Firstly, laser processing of spots was performed to identify the ablation thresholds for WC-Co and Co phase individually. Subsequently, laser processing of lines and square regions was conducted using the selected process parameter range. Pulse energy was varied between 3.1 µJ and 12.6 µJ, depending upon the experimental study whereas a scanning speed (ν) between 50 – 2000 mm/s was examined. For all experiments, the pulse repetition rate (PRR) was kept constant as 500 kHz. Table 1 summarizes the range of process parameters for the different morphologies fabricated. Pulse overlap (*PO*) between successive pulses during scanning is calculated [11] using, $PO\ (\%) = [1 - (\nu/(d_f \times PRR))] \times 100$ for different scanning speeds and included in Table 1.

Surface morphology of the laser processed surfaces was observed by field emission scanning electron microscopy (FESEM, XL30 FEG, FEI) and high-resolution SEM (NanoSEM, Nova 450, FEI). The distribution of elements, determined by wavelength dispersive X-ray analysis (WDS) of a representative microstructure was performed by electron

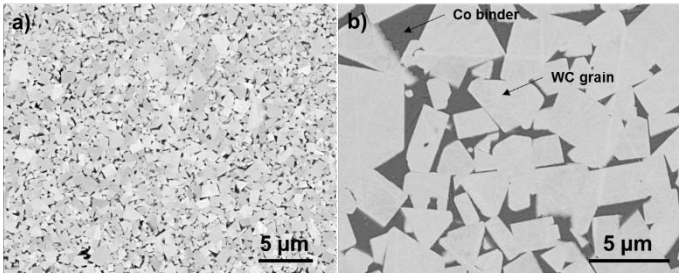

Fig. 1. Microstructure of (a) MG12 (WC-6%wt Co) and (b) GC32 (WC-10%wt Co).

Table 1. Process parameters used for femtosecond laser processing (FLP)

Process parameter	Spots	Lines	Square region
Laser pulse energy (E_p) (µJ)	3.1,3.6,4.1,…,12.6	4.1,4.2,4.4	3.8,3.9,4.1,4.2,4.4,4.6
Pulse repetition rate (*PRR*) (kHz)	500	500	500
Number of pulses (*N*)	1, 2, 5, 10, 20	N.A	N.A
Scanning speed (v) (mm/s)	N.A	50, 100, 200, 400, 800, 1600	600, 1600, 2000
Pulse overlap (*PO*) (%)	N.A	99.4, 98.8, 97.5, 95, 90, 80	92.5, 80, 75
Hatch spacing (µm)	N.A	N.A	5
Material investigated	MG12 (WC-6%wt Co)	MG12 (WC-6%wt Co)	GC32 (WC-10%wt Co)

probe microanalysis (EPMA, JXA-8530F, JEOL Ltd, Japan). The beam current and accelerating voltage were fixed at 50 nA and 15 kV.

3. Results and discussions

3.1. FLP of spots

In this section, spots were fabricated on MG12 at varying pulse energy and number of pulses. Fig. 2 compares the single pulse ablation of spots at different laser pulse energies. No visible ablation on the processed surface was observed for a pulse energy between 3.1 µJ (not shown) and 4.6 µJ (Fig. 2a). At 5 µJ, signs of ablation in the form of valleys dispersed randomly in the processed zone can be noticed in Fig. 2b. Elemental analysis at the corresponding surface (shown in Fig. 3a) reveals that the valleys have a reduced W content, indicating the possible removal of WC grains during processing. Typically, ablation of the Co binder phase occurs first during the *fs* laser irradiation due to its lower melting and boiling temperatures. In addition to the poor stability of the grains without the binder, the evaporation of Co could also lead to the removal of WC grains. A slight increase in Co content noticed in the valleys highlight the phenomenon of Co binder removal from the surface and ejection of WC grains rather than the ablation of WC at low pulse energies.

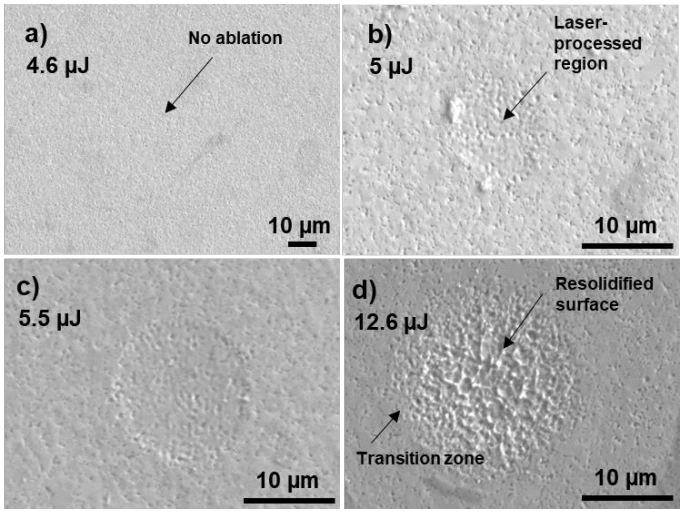

Fig. 2. Single pulse *fs* laser processing of spots at different pulse energy on MG12: (a) 4.6 µJ; (b) 5 µJ; (c) 5.5 µJ; (d) 12.6 µJ.

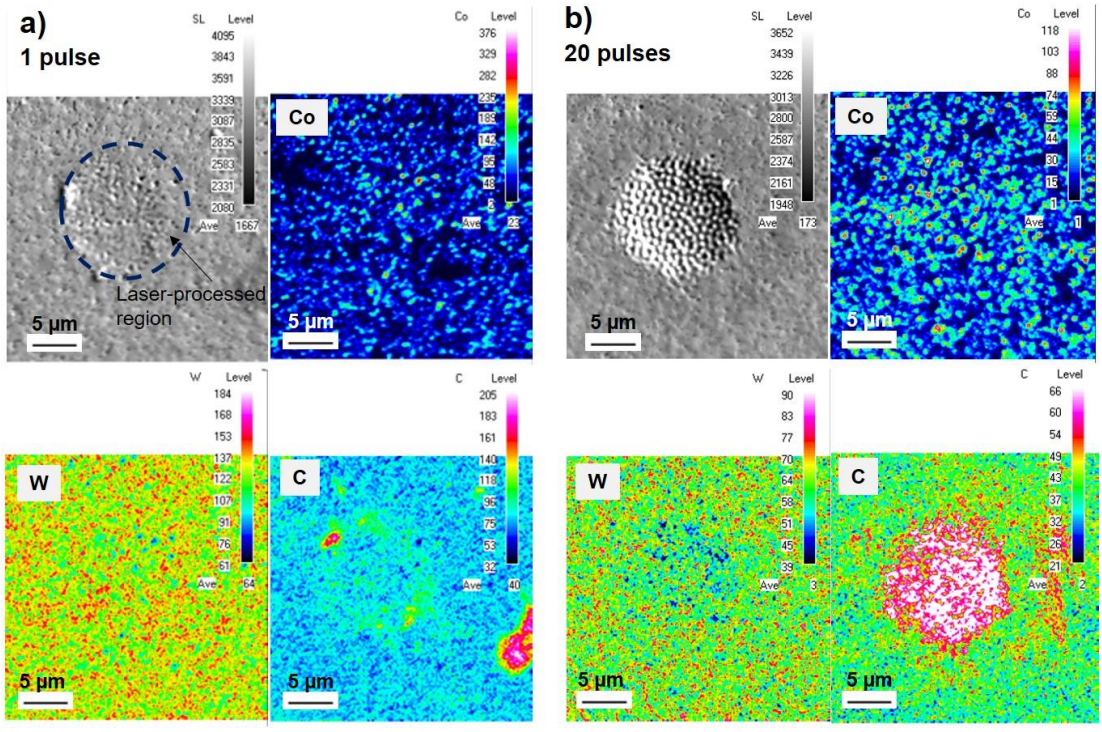

Fig. 3. Elemental distribution of laser ablated spots at 5 µJ for MG12: (a) 1 pulse; (b) 20 pulses

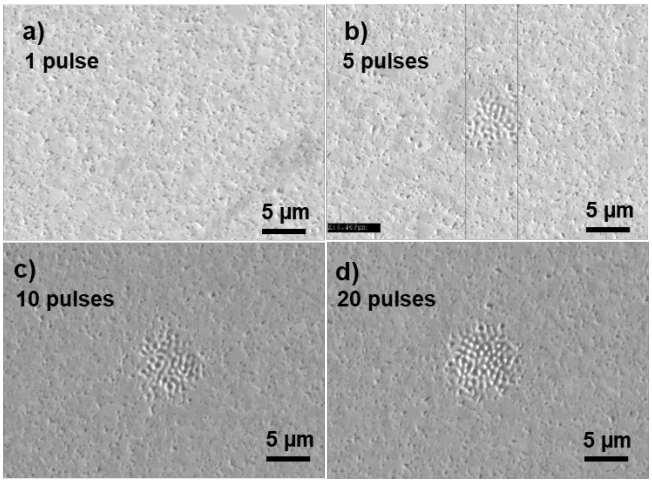

Fig. 4. FLP of spots after a different number of pulses on MG12: (a) 1; (b) 5; (c) 10; (d) 20. [pulse energy = 4.6 µJ]

With the further increase in pulse energy, the ablation area increases gradually with the formation of clear edges (Fig. 2c) before experiencing the eutectic melting and solidification of WC and Co grains at 12.6 µJ (Fig. 2d). In comparison to the laser ablation with *ns* lasers [6,9,12], a *fs* laser ablation of WC shows no redeposited crown-like edge structures, blow holes, pores or large HAZ.

Fig. 4 illustrates the effect of the number of pulses on laser ablation of WC at a constant pulse energy of 4.6 µJ. The laser-processed spots consist of valleys, whose depth increases with the number of pulses. Previous studies with *ns* pulses/CW laser [6,12] reported the formation of hills and valleys made of WC and Co, respectively. Li et al. [6] postulated that only Co was ablated during laser processing whereas the hills represent non-ablated WC. Arroyo et al. [12] observed that complete melting and subsequent solidification of WC along with the vapor expansion could also lead to WC hills and Co valleys. However, the size of the resultant WC peaks after laser ablation in those studies [6,12] was larger than 5 µm. The observed behaviour in Fig. 4 is different as there is no WC grain growth.

The possible mechanism corresponding to *fs* laser processing in this study can be explained as follows: during the initial laser pulses, the Co binder at the surface layer is ablated leaving WC grains unaffected. Upon subsequent pulses, there is more laser absorption at the ablated regions leading to increased Co removal and deepening of the valleys. At this stage, the surface is dominated by WC grains. During further laser irradiation, there is more laser energy at the WC grain boundaries due to the multiple beam reflections at the neighbouring valleys [7], which could lead to subsequent melting and solidification of WC generating rounded WC edges. It can be concluded from this section that a laser pulse energy below 4.6 µJ, corresponding to a sample morphology without visible ablation, should be used to selectively remove the Co phase.

3.2. FLP of lines

In this section, FLP of a line morphology is conducted at optimized laser pulse energies in the range 4.1-4.4 µJ and at varying scanning speeds. Fig. 5 compares the laser processed lines at a pulse energy of 4.2 µJ for scanning speeds ranging between 50 and 1600 mm/s (corresponding to pulse overlap between 99.4% and 80%). At a low scanning speed of 50 mm/s (99.4% *PO*), the Co binder is found to be fully ablated whereas WC grain boundaries are becoming clearly visible (Fig. 5a) as blunt boundaries. Fig. 6a shows the microstructure at the same scanning speed but at a slightly higher pulse energy (4.4 µJ). It can be noticed that the surface morphology is comprised of large peaks with rounded edges, signifying the melting and solidification of WC grains during FLP. The growth of WC grains in Fig. 6a is also obvious as the peaks approximately have a size of 1 µm compared to the initial WC grain size (0.5 µm).

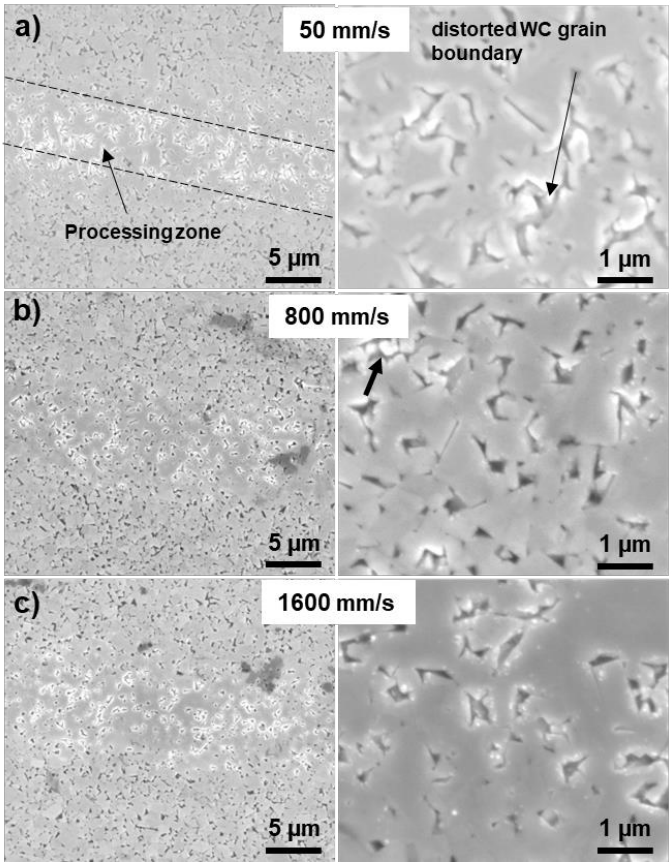

Fig. 5. FLP of lines at different scanning speed on MG12: a) 50 mm/s (99.4 % PO) ; b) 800 mm/s (90 % PO); c) 1600 mm/s (80 % PO) [pulse energy = 4.2 µJ]

With an increase in scanning speed to 800 mm/s and reduced pulse overlap to 90%, only the Co binder is ablated from the surface, as shown in Fig. 5b. However, the WC grain boundary is still slightly distorted at a few locations (see, arrow in Fig. 5b), possibly due to a lack of binding of WC grains with the Co removal. When the scanning speed is increased further to 1600 mm/s, the binder seems to be fully removed from the surface while retaining the sharpness of the WC grain boundary due to the reduced pulse overlap (80%) and the corresponding energy density, as shown in Figs. 5b and 6b. Redeposition of ablated nanoparticles can be seen in Figs. 5 and 6 for all processing conditions.

3.3. FLP of square regions

In this section, FLP was conducted on GC32, a coarser and higher Co content WC-Co grade (average grain size of 2.16 µm), using the parameters optimized in sections 3.1 and 3.2, for comparison. Fig. 7 compares the surface morphology of GC32 at different scanning speeds for a pulse energy of 4.6 µJ. At a low scanning speed of 600 mm/s, a WC grain morphology with rounded edges (Fig. 7a) is observed due to the higher energy density achieved by a higher pulse overlap of 92.5%.

For an increasing scanning speed, ablation occurs only at the Co binder with no noticeable melting and solidification of WC grains. Although WC is shown to retain its sharp grain boundaries at higher scanning speeds, cracking of WC grains is also observed at multiple locations (Fig. 7b). With a further increase in scanning speed to 2000 mm/s, a reduction in crack formation was observed due to reduced *PO* (80%) and energy density, as shown in Figs. 7c and 7d. During laser irradiation of WC-Co, rapid cooling of WC leads to the formation of thermal stresses and cracks typically in the resolidified WC layer [13]. In this study, cracks are observed on the WC grains without any evident melting and evaporation of WC. WC can experience localized heating and thermal stresses due to the difference in thermal properties (thermal conductivity, coefficient of thermal expansion) between WC and Co phases [7,14]. In a study on *fs* laser processing of different carbides with varying grain sizes to produce periodic textures, Lian et al. [15] found that a coarser grained microstructure resulted in

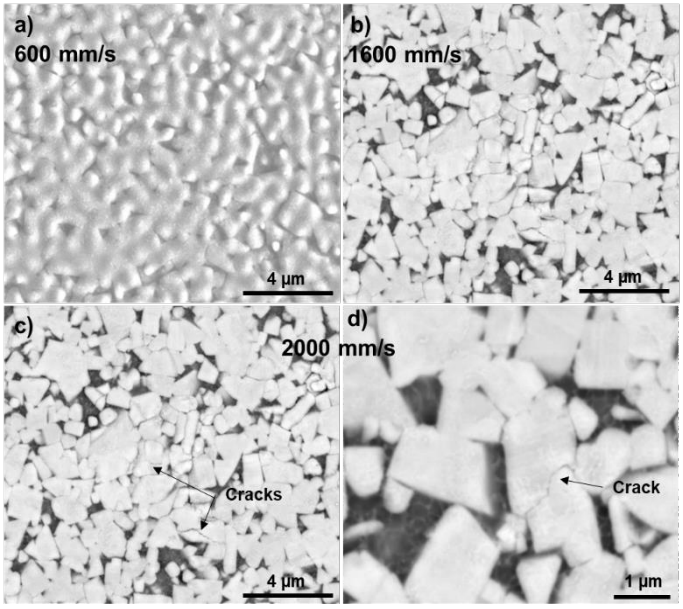

Fig. 7. FLP of square regions at different scanning speed on GC32: a) 600 mm/s (92.5 % PO); b) 1600 mm/s (80 % PO); c) and d) 1600 mm/s (80 % PO) [pulse energy = 4.6 µJ]

an increased quantity of cracks and holes. As GC32 has larger WC grains compared to MG12, the crack formation could be more prominent in GC32. Despite a minimal heat-affected

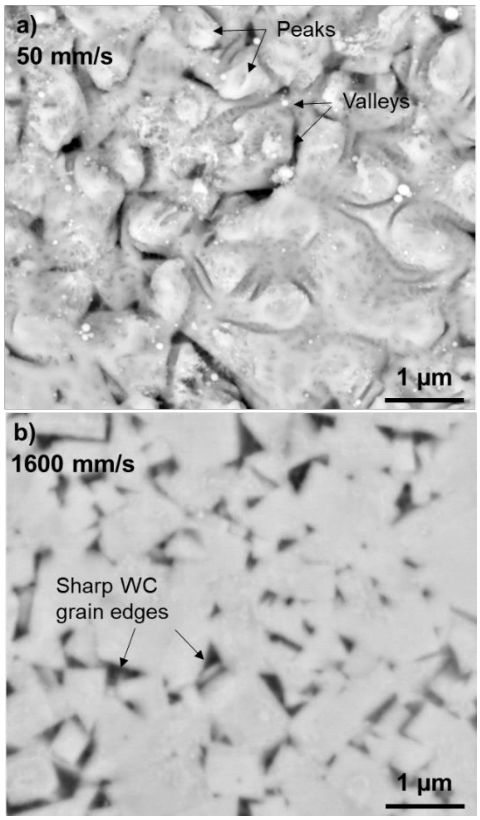

Fig. 6. Surface morphology after FLP at different scanning speed; a) 50 mm/s (99.4 % PO); b) 1600 mm/s (80 % PO) [pulse energy = 4.4 µJ]

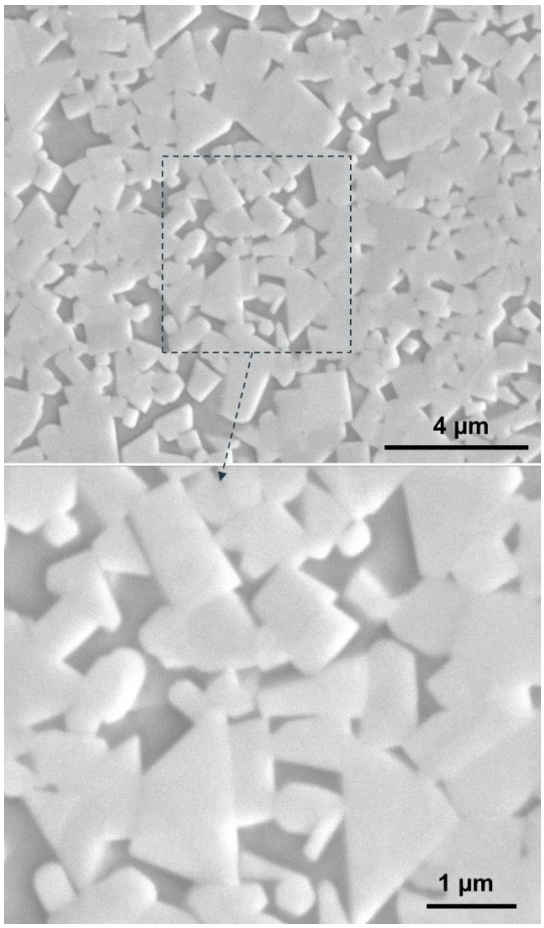

Fig. 8. Surface morphology of GC32 after FLP at 3.8 µJ and 600 mm/s (92.5% PO)

zone, *fs* laser processing could still result in the formation and expansion of cracks due to an induced thermal residual stress.

Fig. 8 shows the surface morphology of GC32 at a lower pulse energy of 3.8 µJ and scanning speed of 600 mm/s. At this processing condition, the Co binder seems to be removed from the surface which can be identified by the deeper pockets between the WC grains. Furthermore, WC grain boundaries retain their sharpness, as seen clearly in Fig. 8. The qualitative results from this study indicate that *fs* laser processing is able to remove the Co binder selectively from the WC-Co surface without affecting the sharpness and size of the WC grains.

4. Conclusions

Femtosecond laser processing has been investigated in this study for the selective removal of the cobalt binder from tungsten carbide-cobalt hardmetal surfaces. Three different morphologies (spot, line and square) have been fabricated using *fs* laser processing. The influence of process parameters such as pulse energy, number of pulses and scanning speed on the microstructure were assessed. The following conclusions can be drawn from the qualitative analysis of the microstructure of the processed surfaces:

- Laser ablation of spots resulted in hills and valleys on the processed surface for pulse energies above 5 µJ. Elemental analysis revealed that the valleys have a reduced W content, indicating potential WC grain removal due to the ablation of the surrounding Co binder. With an increasing number of pulses, Co ablation increased leading to deeper valleys with rounded WC grain boundaries.
- In general, FLP of WC-Co shows no redeposited edge structures, blow holes, pores or large HAZ which are typically observed with *ns* laser ablation.
- After FLP of line morphologies at low scanning speeds, the surface morphology is comprised of large peaks with rounded edges, indicating eutectic melting and resolidification of WC grains in addition to WC grain growth. FLP of MG12 at a higher scanning speed (1600 mm/s) and optimized pulse energy (4.2 µJ) however resulted in the selective removal of Co binder while retaining the sharpness of the WC grain boundaries.
- For similar pulse energy (4.2 – 4.6 µJ), FLP of GC32 experienced selective Co ablation and no WC grain boundary damage but there was crack formation on the WC grains without any evident melting and evaporation. This could be attributed to the larger WC grain size of GC32 and thermal residual stresses. Under optimum process conditions (3.8 µJ and 600 mm/s), selective Co phase removal from GC32 WC-Co surfaces without modification of the WC grain size and morphology could be achieved.

Quantitative elemental analysis of the surface and cross-sections of the *fs* laser processed surfaces will be further investigated.

Acknowledgements

This research was supported by Internal Funds of KU Leuven through C3 IOF project C3/20/084.

References

[1] Dumpala R, Chandran M, Ramachandra Rao MS. Engineered CVD Diamond Coatings for Machining and Tribological Applications. JOM. 2015;67(7):1565–77.
[2] Inspektor A, Oles EJ, Bauer CE. Theory and practice in diamond coated metal-cutting tools. Int J Refract Met Hard Mater. 1997;15(1–3):49–56.
[3] Polini R, Bravi F, Casadei F, D'Antonio P, Traversa E. Effect of substrate grain size and surface treatments on the cutting properties of diamond coated Co-cemented tungsten carbide tools. Diam Relat Mater. 2002;11(3–6):726–30.
[4] Raghuveer MS, Yoganand SN, Jagannadham K, Lemaster RL, Bailey J. Improved CVD diamond coatings on WC-Co tool substrates. Wear. 2002;253(11–12):1194–206.
[5] Kamiya S, Takahashi H, Polini R, D'Antonio P, Traversa E. Effect of WC-Co substrates pre-treatment and microstructure on the adhesive toughness of CVD diamond. Diam Relat Mater. 2001;10(3–7):786–9.
[6] Li T, Lou Q, Dong J, Wei Y, Liu J. Selective removal of cobalt binder in surface ablation of tungsten carbide hardmetal with pulsed UV laser. Surf Coatings Technol. 2001;145(1–3):16–23.
[7] Barletta M, Rubino G, Gisario A. Co removal and phase transformations during high power diode laser irradiation of cemented carbide. Appl Surf Sci. 2011;257(9):4239–45.
[8] Han J, Malek O, Vleugels J, Braem A, Castagne S. Ultrafast laser selective phase removal for surface modification of nanocomposite materials. Opt Express. 2021;29(16):24834.
[9] Fang S, Soldera F, Rosenkranz A, Herrmann T, Bähre D, Llanes L. Microstructural and Metallurgical Assessment of the Laser-Patterned Cemented Tungsten Carbide (WC-CoNi). In: Procedia Manufacturing. Elsevier B.V.; 2018. p. 198–204.
[10] Fang S, Müller DW, Rauch C, Cao Y, Mücklich F, Llanes L. Fabrication of Interference Textures on Cemented Carbides Using Nanosecond and Femtosecond Laser Pulses. In: Procedia CIRP. Elsevier B.V.; 2020. p. 216–21.
[11] Schnell G, Duenow U, and Seitz H. Effect of laser pulse overlap and scanning line overlap on femtosecond laser-structured Ti6Al4V surfaces. Materials, 2020; 13(4): p. 969.
[12] Arroyo JM, Diniz AE, de Lima MSF. Cemented carbide surface modifications using laser treatment and its effects on hard coating adhesion. Surf Coatings Technol. 2010;204(15):2410–6.
[13] Yilbas BS, Arif AFM, Karatas C, Ahsan M. Cemented carbide cutting tool: Laser processing and thermal stress analysis. Appl Surf Sci. 2007;253(12):5544–52.
[14] Neves D, Diniz AE, Lima MSF. Microstructural analyses and wear behavior of the cemented carbide tools after laser surface treatment and PVD coating. Appl Surf Sci. 2013;282:680–8.
[15] Lian Y, Deng J, Yao B, Zhuo Y, Lei S. Influence of different cemented carbides on fabricating periodic micro-nano textures by femtosecond laser processing. Surf Coatings Technol. 2017;317:166–71.